Strain effect in determining the geometric shape of self-assembled quantum dot

2009 J. Phys. D: Appl. Phys. 42 125414

(http://iopscience.iop.org/0022-3727/42/12/125414)

J. Phys. D: Appl. Phys. **42** (2009) 125414 (8pp) doi:10.1088/0022-3727/42/12/125414

Strain effect in determining the geometric shape of self-assembled quantum dot

X-F Yang[1,2], K Fu[1], W Lu[2], W-L Xu[3] and Y Fu[1]

[1] Department of Theoretical Chemistry, School of Biotechnology, Royal Institute of Technology, S-106 91 Stockholm, Sweden
[2] National Lab for Infrared Physics, Shanghai Institute of Technical Physics, Chinese Academy of Sciences, 500 Yutian Road, Shanghai 200083, People's Republic of China
[3] Department of Information Science and Technology, East China Normal University, North Zhongshen Road 3663, Shanghai 200062, People's Republic of China

Received 13 October 2008, in final form 8 May 2009
Published 5 June 2009
Online at stacks.iop.org/JPhysD/42/125414

Abstract
The geometric shape of a self-assembled quantum dot (QD) formed by the strain-induced Stranski–Krastanov mode has been studied as a function of strain energy by the short-range valence-force-field approach. It has been shown by dynamic bond relaxation through strain energy minimization that for the most commonly used InAs QD in GaAs and InP matrices and Ge QD in Si matrix, a pyramidal shape is energy favoured over an hemispherical shape when the QD is not capped due to the lattice relaxation at the QD surface. When the QD becomes totally embedded in the background material, the elastic strain energy of a hemispherical InAs QD is minimal. The results agree with experimental observations. We further studied the coupling of strain fields of QDs in adjacent QD layers which shows that QDs in multiply stacked QD layers can be aligned along the layer growth direction in order to minimize the strain energy.

(Some figures in this article are in colour only in the electronic version)

1. Introduction

Self-assembled semiconductor quantum dots (QDs) formed by the strain-induced Stranski–Krastanov (SK) mode have been extensively studied, developed and applied in electronics and optoelectronics. These QD structures are formed following a strained coherent islanding in heteroepitaxial systems so that strain energy is expected to be an important factor in the QDs' self-assembling process [1–4]. The four most common geometric structures, hemispheres (dome-shaped) of InAs QD in GaAs matrix, abbreviated as InAs/GaAs [5–9], InAs/InP [10] and Ge/Si [11], pyramids of CdTe/ZnTe [12], Ge/Si [1, 13], truncated pyramids of SiGe/Si [14], InAs/GaAs and InGa/InP [15] and multiple-bounding facets of InAs/GaAs [16–18], are shown in figure 1. There are also other forms, e.g. truncated cones of InGaAs/GaAs [19] and InAs/InP [20]. Atomically resolved scanning tunnel microscopy, atomic force microscopy as well as scanning near-field electron beam induced current microscopy measurements are commonly performed to characterize the QD structures at the atomic level. Geometric shapes of the uncapped QDs appear to be mostly pyramids with multiple facets, whereas hemispherical smooth surfaces were normally reported for QDs that are totally embedded in heterosemiconductor backgrounds.

Furthermore, multiple QD layers have been stacked vertically for achieving the high spatial density that is necessary for device applications [21–23]. Strain interactions between QD layers were experimentally demonstrated [24] and utilized to control lateral spacing and vertical alignment of multiple self-assembled InAs QD layers in GaAs background material [25].

The geometric shape of the QD is determined by many factors including growth conditions and inter-diffusion between QD material and background material. By a hybrid computational approach that combines continuum calculations of strain energy with first-principles results, relatively small effects associated with surface stress were obtained for InAs/GaAs system [26], while it was theoretically demonstrated to be an important factor in Ge/Si QD formation [27]. Wise *et al* demonstrated the evolution of the QD formation under the strong influence of surface energy by cubic elastic equilibrium equations [28]. Recent kinetic Monte Carlo study of metal organic chemical vapour deposition (MOCVD) growth mechanism of GaSb QDs in GaAs showed that the

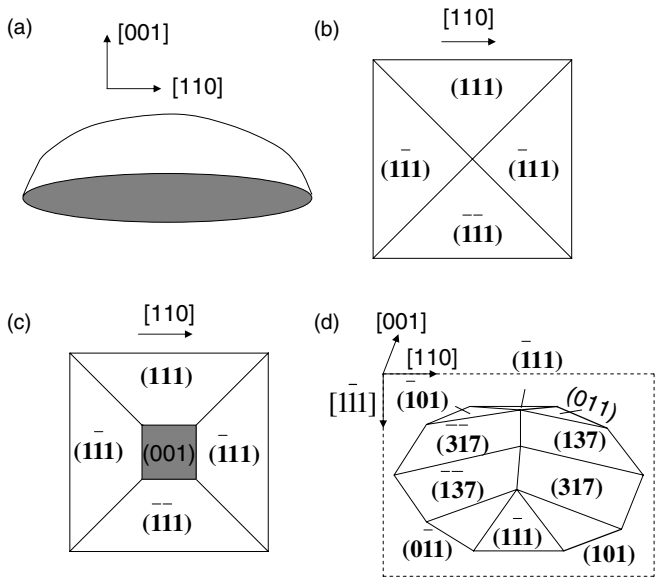

Figure 1. Four common geometric structures of self-assembled QDs: (*a*) hemisphere, (*b*) pyramid, (*c*) truncated pyramid and (*d*) multiple-bounding facets.

strain induced by the lattice mismatch between the epitaxial material and the substrate is directly responsible for the QD formation and the transition from two-dimensional to three-dimensional growth mode [29]. Note that [26] was based on the *ab initio* study (density functional theory, DFT), while the continuum elasticity theory was adopted for the long-range strain fields to account for the strain relaxations. When the DFT theory is used, lattice re-constructions including surface relaxations are normally accounted for. This can be a possible reason to understand results of [26] that the extra inclusion of the strain field has a limited effect.

In this work we apply the short-range valence-force-field (VFF) approach to describe inter-atomic forces in the QD systems in terms of bond stretching and bending [30, 31]. The model is microscopic and has been widely applied in bulk and alloys [32–37], as well as low-dimensional systems [38–40]. In the VFF model, the deformation of a lattice structure is completely specified when the location of every atom in the system is given [30], and the elastic energy of a bond is minimal in its three-dimensional relaxed bulk lattice structure. We will study the geometric shape of self-assembled QD as a function of strain field (including strain-field-induced reconstruction of surface atoms) to understand quantitatively experimental results. Coupling between strain fields of adjacent QD layers will also be investigated for designing multiple QD layer stacking necessary for device applications.

Section 2 describes the VFF models for materials of zinc blende group III–V and IV. Numerical results and discussions about single QD will be presented in section 3. Section 4 concentrates on the coupling between strain fields of adjacent QD layers. A brief summary is given in section 5.

2. Theoretical analyses and discussions of single QD

For small deformations, the elastic energy of an inter-atomic bond can be written as a Taylor expansion in bond length variation and variations in the angles between the bond and its nearest-neighbour bonds. By following the general notations of [32–34, 41], the elastic energy of one inter-atomic bond can be written in the harmonic form as

$$E_i = K_{ir}\delta r_i^2 + K_{i\Omega} r_{i0}^2 \sum_j \delta\Omega_{ij}^2 + K_{irr}\delta r_i \sum_j \delta r_j, \quad (1)$$

where j denotes the nearest-neighbour bonds. δr_i is the variation of the length of bond i, $\delta\Omega_{ij}$ is the variation of the angle between bond i and j, r_{i0} is the length of bond i in its relaxed format. The total elastic energy is the sum of all bond energies:

$$E_{\text{elastic}} = \sum_i E_i. \quad (2)$$

Numerical values of K for VFF bonds of zinc blende bulk materials are listed in table 1 obtained from elastic coefficients C_{11}, C_{12} and C_{44} by equalizing the strain energies of bulk materials under hydrostatic pressure and sheer stress, using the VFF model and the continuum medium model (C values [42–44]). More specifically, we consider a bulk semiconductor under a hydrostatic pressure and a sheer stress along the x direction. The bulk semiconductor is composed of N unit cells in the x, y and z directions so that its lengths are all Na and volume $(Na)^3$. Under a hydrostatic pressure, the sizes of the semiconductor are modified by δ_x, δ_y and δ_z so that the displacements of each atom are

$$u = \frac{x}{Na}\delta_x, \qquad v = \frac{y}{Na}\delta_y, \qquad w = \frac{y}{Na}\delta_z, \quad (3)$$

by which we can easily obtain the geometric modifications of inter-atomic bonds and thus the total bond energy. On the other hand, the continuum medium approximation gives the strain field distribution

$$\varepsilon_{xx} = \frac{\partial u}{\partial x} = \frac{\delta_x}{Na}, \qquad \varepsilon_{yy} = \frac{\delta_y}{Na}, \qquad \varepsilon_{zz} = \frac{\delta_z}{Na} \quad (4)$$

due to the hydrostatic pressure. For zinc blende structures, the stress fields are

$$\begin{aligned} \sigma_{xx} &= C_{11}\varepsilon_{xx} + C_{12}\varepsilon_{yy} + C_{12}\varepsilon_{zz}, \\ \sigma_{yy} &= C_{21}\varepsilon_{xx} + C_{11}\varepsilon_{yy} + C_{12}\varepsilon_{zz}, \\ \sigma_{zz} &= C_{21}\varepsilon_{xx} + C_{12}\varepsilon_{yy} + C_{11}\varepsilon_{zz}. \end{aligned} \quad (5)$$

Other components of ε and σ are zero so that the strain energy is

$$E_{\text{elastic}} = \tfrac{1}{2}[C_{11}(\varepsilon_{xx}^2 + \varepsilon_{yy}^2 + \varepsilon_{zz}^2) + 2C_{12}(\varepsilon_{xx}\varepsilon_{yy} + \varepsilon_{xx}\varepsilon_{zz} + \varepsilon_{yy}\varepsilon_{zz})](Na)^3. \quad (6)$$

Table 1. Lattice constant a, elastic coefficients C [42–44] and K of zinc blende InAs, InP, GaAs, Si and Ge bulk materials at 100 K.

	InAs	InP	GaAs	Ge	Si
a (Å)	6.05	5.86	5.65	5.657	5.432
C_{11} (GPa)	83.29	101.1	122.1	128.9	165.7
C_{12} (GPa)	45.26	56.1	56.6	48.3	63.9
C_{44} (GPa)	39.59	45.6	60.0	67.1	79.6
K_r (GPa Å)	170.13	198.57	215.09	212.4	256.1
K_Ω (GPa Å)	9.59	10.99	15.41	18.9	23.1
K_{rr} (GPa Å)	59.32	71.14	74.85	73.2	93.2

For the sheer stress along the x direction of $u = z \tan\theta$, $v = 0$ and $w = 0$ for which

$$\varepsilon_{xy} = \tfrac{1}{2}\tan\theta,$$
$$\sigma_{xy} = \tfrac{1}{2}C_{44}\tan\theta, \qquad (7)$$
$$E_{\text{elastic}} = \tfrac{1}{8}C_{44}\tan^2\theta(Na)^3.$$

We can further consider another sheer stress along the y direction so that we totally have three independent linear equations for K_{ir}, $K_{i\Omega}$ and K_{irr}. Note that K values depend on the temperature of the material due to the temperature dependence of the lattice constant. The dependence, however, is found to be very weak. The K values listed in table 1 are obtained for bulk materials at 100 K.

3. Single QD

We consider an inhomogeneous system including totally 1.8 million zinc blende atomic sites in the form of approximately a spherical ball with a radius of $130 \times a/4$ (for the lattice construction in the numerical simulation see [45]). We consider two types of QDs, one is self-assembled on a semi-infinite substrate (without capping) and the other is completely embedded in the substrate material. The QD atoms are positioned in the middle of the cluster. All atoms in the initial lattice system assume the lattice positions of background bulk material. The spatial coordinates of all atoms involved in the numerical calculation are adjusted with respect to the strain energy using a Monte Carlo scheme in which we generate random walkings for all atoms which will only be effective when the elastic energy is reduced after the random walkings. During such a dynamic strain energy minimization process, the random walking step size decreases gradually. Figure 2 shows the total elastic energies of two pyramid InAs/GaAs QDs. Discontinuities in the elastic energy evolution are observed at an interval of 10 000 random walking steps at which the step size is reduced by a factor of 10. Figure 2 shows that the elastic energy of the uncapped QD is significantly smaller than the buried QD because of the lattice relaxations of atoms at the QD surface.

We consider zinc blende InAs QDs in GaAs and InP matrices and Ge QD in Si matrix, which have been extensively studied in the literature. The K values for InAs/GaAs and InAs/InP systems are defined for all inter-atomic bonds. The Ge–Si bonds in the Ge/Si systems are however, not defined in table 1 which are approximated by averaging the Si–Si and Ge–Ge bonds. For the four QD shapes of figure 1 under investigation, the aspect ratio of the hemisphere is the smallest, only 0.1. It is 0.15 for multiple-bounding facets, 0.25 for truncated pyramid, while the pyramid has the highest value of 0.5. We study three QD volumes of 11.4, 34.5 and 91.3 nm^3 for each QD shape (note that the aspect ratios of these different-volume QDs with the same shape are kept constant), the strain energy per QD atom (i.e. atoms that are inside the QD) is presented in figure 3. For Ge QDs, the strain energy of pyramid is always minimal with respect to the pseudo-situation of strain-free Ge–Si heterostructure for these small

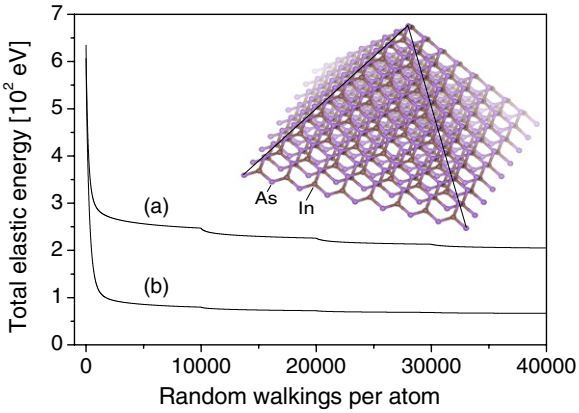

Figure 2. Total elastic energies of InAs QD pyramids (volume = 11.4 nm^3), one embedded in GaAs matrix (a) and the other on a semi-infinite GaAs substrate (b). The inset shows the lattice structure of a miniature InAs QD pyramid.

sizes under investigation, which agrees well with experimental observation about the small-volume Ge islands on Si [1, 46]. However, for some of the sizes the strain energies of pyramids are very similar to those of truncated pyramids. InAs QD pyramid is favoured over hemisphere when the QD is not capped. The strain energy of hemispherical InAs QD becomes the smallest when the QD is totally embedded in the GaAs substrate material. These results also agree with experimental observations [5, 8, 16, 18]. Note that in InP substrate the result of InAs QD depends on the QD size. The differences among InAs/GaAs, InAs/InP and Ge/Si QDs are due to the degree of lattice mismatch, which is $6.05/5.65 - 1 = 0.07$ for InAs/GaAs, 0.03 for InAs/InP and 0.04 for Ge/Si.

We observe a strong dependence of the strain energy on the QD size for the sizes under investigation. The principal reason is the strain relaxation that our QDs are relatively small so that most QD atoms have the possibility to relax (especially those surface atoms) so that the total strain energy can be significantly released. Such relaxation is stronger in the uncapped QDs because of the surface atoms on the uncapped side, see figure 2. Figure 3 shows that the increase in the strain energy following the increase in the QD volume becomes small for large QDs, especially for the uncapped QDs. We can envisage a more or less saturated strain energy per QD atom for large QDs where the ratios between the numbers of surface QD atoms and total QD atoms become small. The contributions from the surface atoms are clearly reflected in the spatial distribution of the strain energy (see figure 4 and its discussions). We have thus far reached our computation limit, so are not able to calculate large QDs. It is, however, strongly believed that the current calculations are highly relevant since these QDs are self-assembled, small initial energy means large possibility of the corresponding final form.

Figure 3 shows that the strain energy in general is large when the aspect ratio is small. Shapes and facets, however, also affect the strain energy, especially for small QDs when the ratios between the surface atoms and total atoms of the QDs are not small. We interpret the effect by considering the following growth pathway: one atom located

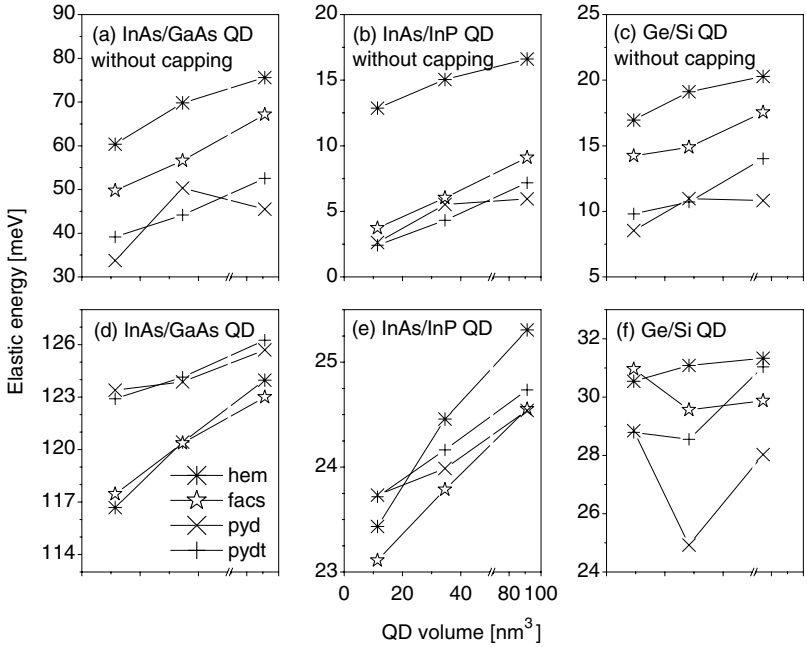

Figure 3. Strain energy per QD atom. (*a*)–(*c*) QDs without capping; (*d*)–(*f*) buried QDs. hem = hemisphere; pyd = pyramid; pydt = truncated pyramid; facs = multi-bounding facets; see figure 1.

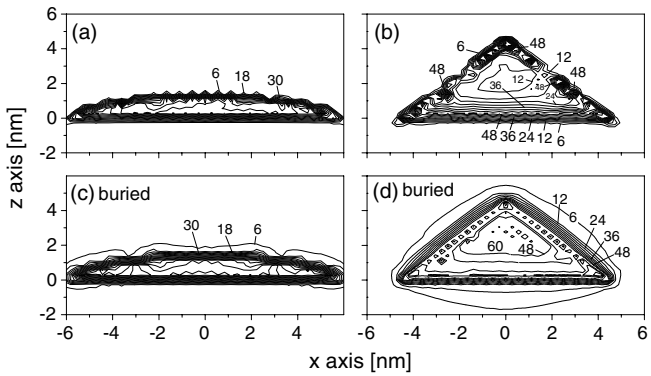

Figure 4. Spatial distributions of strain energies around InAs QDs (volume = 91.3 nm^3) in GaAs matrices; $y = 0$. Linear scale applies and values associated with contour lines are in the unit of meV.

at $(0, 0, 0)$ on a growing surface. It is bounded to two nearest neighbours underneath the growing surface, located at $\frac{a}{2}(1, 1, -1)$ and $\frac{a}{2}(-1, -1, -1)$, where a is the lattice constant of the zinc blende crystal. (The other two nearest neighbours $\frac{a}{2}(1, -1, 1)$ and $\frac{a}{2}(-1, 1, 1)$ have not been grown yet.) For this atom, the displacement (adjustment of its spatial position) is preferred to be along the $[1, 1, 0]$ direction in order not to twist the lattice structure, thus minimizing the local strain energy.

The spatial distributions of the strain energies around InAs/GaAs QDs are presented in figure 4. The strain energy of the QD pyramid is significantly small when the QD is uncapped due to the lattice relaxation at the QD surface, whereas atoms in the QD hemisphere are not able to relax much since all of them are very close to the substrate and therefore are significantly strained. This demonstrates clearly the general understanding of the strain-driven self-assembling formation of QDs that the lattice-mismatch-induced strain is largely released when the QD forms on a substrate.

The displacement of every atom and the strain field are obtained by comparing the true spatial position of the atom with its initial one, from which the strain field distribution is readily calculated which are presented in figure 5. The strain fields of the QD hemisphere can be very well approximated by the ones of the InAs quantum well embedded in the GaAs matrix since the horizontal dimension (diameter = 12 nm) is much larger than the vertical one (height = 1.5 nm). Note that this is only true for QDs with relatively small aspect ratios (smaller than 15%). The strain field distribution in the GaAs background is also very significant, especially perpendicular to the substrate surface, which has been reported and utilized experimentally to grow a three-dimensional QD structure [2, 3, 47]. The strain distribution in the QD pyramid is rather complicated. We observe significant strain relaxation inside the QD in the top vicinity. The surrounding background material becomes also largely strained. The major reason is again the ratio between the numbers of the surface and total QD atoms. In other words, the main difference between the hemisphere and pyramid QDs under discussion is the aspect ratio. For the hemisphere QD with a small aspect ratio, surface atoms dominate which are either very close to or in direct contact with the GaAs substrate, whereas atoms in the pyramid QD can be well catalogued into strained surface atoms and much-relaxed bulk ones.

Numerical fluctuations (fine structures) in figures 4 and 5 are due to the discrete nature of the lattice sites. The lattice displacement (u, v, w) in the VFF model is only defined at the discrete lattice sites. Isoparametric element method of interpolation [48] has been adopted to find out (u, v, w) near the lattice site in order to calculate the strain field of $(\epsilon_{xx} = \partial u/\partial x, \epsilon_{yy} = \partial v/\partial y, \epsilon_{zz} = \partial w/\partial z)$.

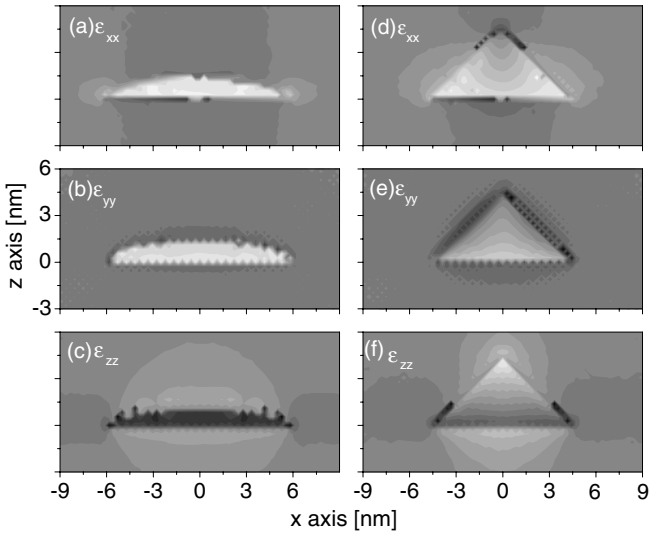

Figure 5. Strain field distributions around InAs QDs embedded in GaAs matrices; $y = 0$. Linear scale from white (-0.04) to black (0.04) applies.

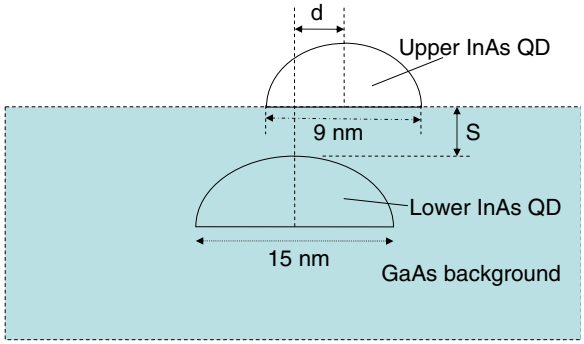

Figure 6. Geometric structure of the coupled QDs.

4. Strain field coupling between adjacent QD layers

We now consider the strain field distribution around two neighbouring self-assembled QDs. As shown in figure 6, the lower InAs QD is totally immersed in the GaAs matrix, with a circular base ($D = 15$ nm) and a vertical aspect ratio of 0.5 (hemisphere), while the upper InAs QD, approached also as a hemisphere, is uncapped, its base is circular (9 nm in diameter). The vertical separation between the two QDs is denoted as s, while the horizontal separation as d.

To simulate the multiple-layer stacking growth mode, we first find the lowest elastic energy field around the lower QD before we deposit the upper QD. The upper QD is then added. Note that the upper QD is not capped for the moment. The total elastic energy after the deposition of the upper QD is shown in figure 7(a). The strain energy increases with the increase in s and d. When the two InAs QDs are far away from each other, the strain energy per In atom converges to the sum of two individual QDs. This effect is not directly observed for the capped dots investigated in figure 7(b). The limit is, however, expected to be reached for a much larger value of the spatial separation due to the more-extended strain field in the GaAs substrate (see figure 4).

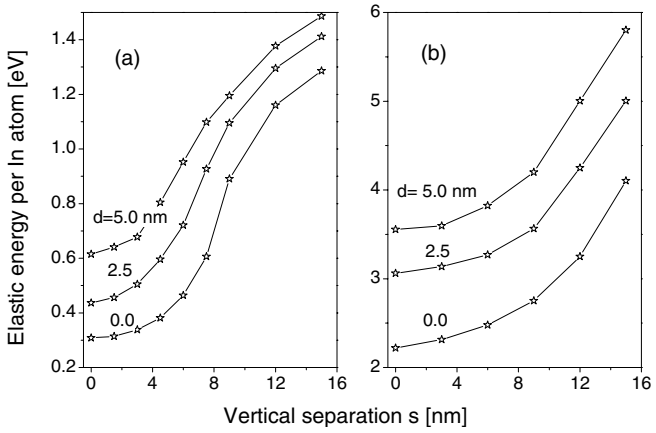

Figure 7. Strain energy per In atom as a function of the QD spatial separation (d and s). (a) The upper InAs QD is not capped and (b) the upper InAs QD is capped.

The spatial distribution of the strain energy around two InAs QDs is presented in figure 8. First of all, we notice the strain at the surface of the GaAs material due to the surface relaxation. Most important of all is the strain energy in the upper InAs QD which is significantly small when the spatial distance between the two QDs is small. This is caused by the strain diffusion from the embedded InAs QD into the surrounding GaAs barrier material. The lattice structure of the GaAs material in the vicinity of the embedded QD becomes partially expanded during the process of strain energy minimization, which reduces its lattice mismatch to the upper InAs QD, thus facilitating the growth of the upper InAs QD. Another important aspect is that the increase in the strain energy as a function of the vertical separation is much slower than the horizontal one. For the vertically aligned QDs (first column in figure 8), the strain energy distribution is not much modified in the upper InAs QD (except at the corners adjacent to the GaAs surface) when we move the embedded QD deeper into the GaAs substrate by 5 nm. This can be utilized to facilitate the vertical alignment of QDs in multiple QD layers for many practical device applications.

The control over the vertical alignment in practice is, however, not easy for the InAs QDs under investigation. The modification in the strain energy due to the change of s from 0.0 to 4.0 nm is very small. It is less than 50 meV in figure 7(a), whereas the growth temperature is about 400–650 °C in the standard MOCVD reactors and molecular beam epitaxy (MBE) systems. Despite the difficulties we still foresee a large possibility of controlling lateral spacing and vertical alignment of self-assembled multiple QD layers by modifying the substrate surface and growth temperature. This was clearly demonstrated experimentally in [24, 25].

We now cap the upper QD by GaAs. As shown in figure 7(b), the strain energy per In atom increases significantly due to the lattice constraint exerted on the surface atoms of the uncapped InAs QD from the capping GaAs material. We, however, observe a similar qualitative relationship between the strain energy and the spatial separation between the neighbouring InAs QDs. The theoretically expected scenario about the multiple-layer stacking growth is therefore that the

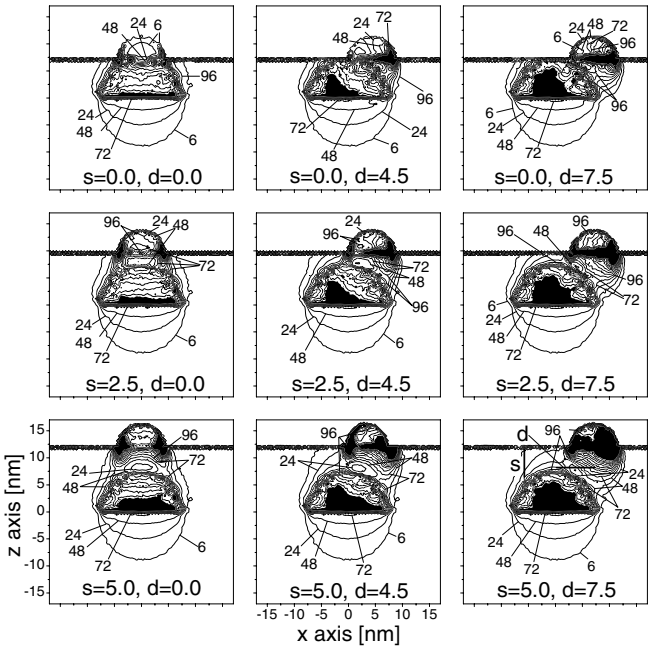

Figure 8. Contour plot of strain energy in the xz plane. Values associated with contour lines are in the unit of meV.

upper InAs QD will be most easily aligned vertically with the lower QD in order to minimize the strain energy. The capping of the upper InAs QD by GaAs will induce a significant new strain field in the upper QD, which will align the QDs in the forthcoming QD layers.

By directly correlating the nucleation rate with the local strain, Tersoff *et al* demonstrated vertical alignment of the QDs; they further showed that the island size and spacing grow progressively more uniform [49]. The local strain was incorporated into a molecular dynamics model which suggests that island nucleation takes place in equilibrium or quasi-equilibrium conditions [50], thus confirms the experimentally observed role of the strain energy in determining the self-assembled QD formation [4, 51]. By the short-range VFF approach to describe inter-atomic forces, our calculations have shown the dominant role of the strain energy in strain-driven QD self-assembling process from the strain energy point of view. It is, however, important to note that other processes could also play important roles in the QD formation. For example, the intermixing processes between the deposited atoms and the substrate ones [51]. Furthermore, under the condition of Si overgrowth, the gradient in the chemical potential across the island was shown to be the most probable driving force for a selective flow of both Ge and Si atoms at the surface which in turn favours the lateral order of QDs [52]. Entropy was shown to play a significant role in the evolution of the size and shape of the Ge–Si islands through the strong thermodynamic drive to form an alloy [53].

5. Summary

In conclusion, we have studied the strain energy of self-assembled QD by the short-range VFF approach to describe inter-atomic forces in terms of bond stretching and bending. The strain-driven self-assembled process of QD based on lattice mismatch has been clearly demonstrated and quantitatively described. It has been shown that due to the lattice relaxation to minimize the strain energy, QD pyramid is energy favoured over hemisphere when InAs QDs in GaAs and InP matrices and Ge QDs in Si matrices are not capped. When the QDs are totally embedded in the background material, the elastic strain energy of a hemispherical InAs QD is minimal. The results agree with the experimental observations.

We further applied the theoretical model to study the multiple-layer stacking growth mode, which shows that the propagation of the strain field from the self-assembled QD to the surrounding substrate material will align the QD formation along the growth direction in order to minimize the strain energy.

Acknowledgments

This work is partially supported by the National Natural Science Foundation of China (Grant No 10474020) and Chinese Key Project for Basic Research (2006CB921507). Computing resources from the Swedish National Infrastructure for Computing (SNIC 001-08-129) are acknowledged.

References

[1] Ross F M, Tersoff J and Tromp R M 1998 Coarsening of self-assembled Ge quantum dots on Si(0 0 1) *Phys. Rev. Lett.* **80** 984–7

[2] Brunner K and Abstreiter G 2001 Ordering and electronic properties of self-assembled Si/Ge quantum dots *Japan. J. Appl. Phys.* **40** 1860–5

[3] Ibáñez J, Patanè A, Henini M, Eaves L, Hernández S, Cuscó R, Artús L, Musikhin Y G and Brounkov P N 2003 Strain relaxation in stacked InAs/GaAs quantum dots studied by Raman scattering *Appl. Phys. Lett.* **83** 3069

[4] Stangl J, Hol V and Bauer G 2004 Structural properties of self-organized semiconductor nanostructures *Rev. Mod. Phys.* **76** 725–83

[5] Miller M S, Malm J-O, Pistol M-E, Jeppesen S, Kowalski B, Georgsson K and Samuelson L 1996 Stacking InAs islands and GaAs layers: strongly modulated one-dimensional electronic systems *J. Appl. Phys.* **80** 3360–4

[6] Fu Y, Ferdos F, Sadeghi M, Wang S M and Larsson A 2002 Photoluminescence of an assembly of size-distributed self-assembled InAs quantum dots *J. Appl. Phys.* **92** 3089–92

[7] Kim H-S, Suh J-H, Park C-G, Lee S-J, Noh S-K, Song J-D, Park Y-J, Choi W-J and Lee J-I 2005 Structure and thermal stability of InAs/GaAs quantum dots grown by atomic layer epitaxy and molecular beam epitaxy *J. Cryst. Growth* **285** 137–45

[8] Ouattara L, Mikkelsen A, Lundgren E, Höglund L, Asplund C and Andersson J Y 2006 A cross-sectional scanning tunneling microscopy study of a quantum dot infrared photodetector structure *J. Appl. Phys.* **100** 44320

[9] Troyon M and Smaali K 2007 Scanning near-field electron beam induced current microscopy: application to III–V heterostructures and quantum dots *Appl. Phys. Lett.* **90** 212110

[10] Carlsson N, Junno T, Montelius L, Pistol M-E, Samuelson L and Seifert W 1998 Growth of self-assembled InAs and

$InAs_xP_{1-x}$ dots on InP by metalorganic vapour phase epitaxy *J. Cryst. Growth* **191** 347–56

[11] Xue F, Qin J, Cui J, Fan Y L, Jiang Z M and Yang X J 2005 Studying the lateral composition in Ge quantum dots on Si(0 0 1) by conductive atomic force microscopy *Surf. Sci.* **592** 65–71

[12] Lee E H, Lee K H, Kim J S and Park H L 2003 Formation and optical properties of CdTe self-assembled pyramids with quantum states grown on ZnTe buffer layers *Appl. Phys. Lett.* **83** 5536–8

[13] Wang C Y, Denda M and Pan E 2006 Analysis of quantum-dot-induced strain and electric fields in piezoelectric semiconductors of general anisotropy *Int. J. Solid. Struct.* **43** 7593–608

[14] Schmidbauer M, Wiebach Th, Raidt H, Hanke M and Köhler R 1998 Ordering of self-assembled $Si_{1-x}Ge_x$ islands studied by grazing incidence small-angle x-ray scattering and atomic force microscopy *Phys. Rev.* B **58** 10523–31

[15] Mikkelsen A and Lundgren E 2005 Cross-sectional scanning microscopy studies of III–V semiconductor structures *Prog. Surf. Sci.* **80** 1–25

[16] Mańquez J, Geelhaar L and Jacobi K 2001 Atomically resolved structure of InAs quantum dots *Appl. Phys. Lett.* **78** 2309–11

[17] Jacobi K 2003 Atomic structure of InAs quantum dots on GaAs *Prog. Surf. Sci.* **71** 185–215

[18] Xu M C, Temko Y, Suzuki T and Jacobi K 2005 On the location of InAs quantum dot on GaAs(0 0 1) *Surf. Sci.* **589** 91–7

[19] Lenz A, Timm R, Eisele H, Hennig Ch, Becker S K, Sellin R L, Pohl U W, Bimberg D and Dähne M 2002 Reversed truncated cone composition distribution of $In_{0.8}Ga_{0.2}As$ quantum dots overgrown by an $In_{0.1}Ga_{0.9}As$ layer in a GaAs matrix *Appl. Phys. Lett.* **81** 5150–2

[20] Ulloa J M, Koenraad P M, Gapihan E, Létoublon A and Bertru N 2007 Double capping of molecular beam epitaxy grown InAs/InP quantum dots studied by cross-sectional scanning tunneling microscopy *Appl. Phys. Lett.* **91** 73106

[21] Heinrichsdorff F, Mao M-H, Kirstaedter N, Krost A, Bimberg D, Kosogov A O and Werner P 1997 Room-temperature continuous-wave lasing from stacked InAs/GaAs quantum dots grown by metal organic chemical vapor deposition *Appl. Phys. Lett.* **71** 22–4

[22] Borgstrom M, Bryllert T, Sass T, Gustafson B, Wernersson L-E, Seifert W and Samuelson L 2001 High peak-to-valley ratios observed in InAs/InP resonant tunneling quantum dot stacks *Appl. Phys. Lett.* **78** 3232–4

[23] Nuntawong N, Birudavolu S, Hains C P, Huang S, Xu H and Huffaker D L 2004 Effect of strain-compensation in stacked 1.3 m InAs/GaAs quantum dot active regions grown by metal organic chemical vapor deposition *Appl. Phys. Lett.* **85** 3050–2

[24] Howe P, Abbey B, Le Ru E C, Murray R and Jones T S 2004 Strain-interactions between InAs/GaAs quantum dot layers *Thin Solid Films* **464–465** 225–8

[25] Lee J H, Wang Z M, Liang B L, Sablon K A, Strom N W and Salamo G J 2007 Multiple vertically stacked quantum dot clusters with improved size homogeneity *J. Phys. D: Appl. Phys.* **40** 198–202

[26] Moll N, Scheffler M and Pehlke E 1998 Influence of surface stress on the equilibrium shape of strained quantum dots *Phys. Rev.* B **58** 4566–71

[27] Shklyaev O E, Beck M J, Asta M, Miksis M J and Voorhees P W 2005 Role of strain-dependent surface energies in Ge/Si(1 0 0) island formation *Phys. Rev. Lett.* **94** 176102

[28] Wise S M, Lowengrub J S, Kim J S, Thornton K and Voorhees P W 2005 Quantum dot formation on a strain-patterned epitaxial thin film *Appl. Phys. Lett.* **87** 133102

[29] Fu K and Fu Y 2008 Kinetic Monte Carlo study of metal organic chemical vapor deposition growth mechanism of GaSb quantum dots *Appl. Phys. Lett.* **93** 101906

[30] Birman J L 1958 Theory of the piezoelectric effect in the zincblende structure *Phy. Rev.* **111** 1510–4

[31] Musgrave M J P and Pople J A 1962 A general valence force field for diamond *Proc. R. Soc. Lond.* A **268** 474–84

[32] Nusimovici M A and Birman J L 1967 Lattice dynamics of wurtzite: CdS *Phys. Rev.* **156** 925–38

[33] Martin R M 1970 Elastic properties of ZnS structure semiconductors *Phys. Rev.* B **1** 4005–11

[34] Ramani R, Mani K K and Singh R P 1976 Valence force fields and the lattice dynamics of beryllium oxide *Phys. Rev.* B **14** 2659–63

[35] Saito T and Arakawa Y 1999 Atomic structure and phase stability of $In_xGa_{1-x}N$ random alloys calculated using a valence-force-field method *Phys. Rev.* B **60** 1701–6

[36] Takayama T, Yuri M, Itoh K, Baba T and Harris J S Jr 2000 Theoretical analysis of unstable two-phase region and microscopic structure in wurtzite and zinc-blende InGaN using modified valence force field model *J. Appl. Phys.* **88** 1104–10

[37] Nabetani Y, Matsumoto T, Sasikala G and Suemune I 2005 Theory of strain states in InAs quantum dots and dependence on their capping layers *J. Appl. Phys.* **98** 63502

[38] Jiang H and Singh J 1997 Strain distribution and electronic spectra of InAs/GaAs self-assembled dots: an eight-band study *Phys. Rev.* B **56** 4696–701

[39] Stier O, Grundmann M and Bimberg D 1999 Electronic and optical properties of strained quantum dots modeled by 8-band $k \cdot p$ theory *Phys. Rev.* B **59** 5688–701

[40] Bernard J E and Zunger A 1991 Strain energy and stability of Si–Ge compounds, alloys, and superlattices *Phys. Rev.* B **44** 1663–81

[41] Keating P N 1966 Effect of invariance requirements on the elastic strain energy of crystals with application to the diamond structure *Phys. Rev.* **145** 637–45

[42] Ito T, Khor K E and Das Sarma S 1989 Empirical potential-based Si–Ge interatomic potential and its application to superlattice stability *Phys. Rev.* B **40** 9715–22

[43] Madelung O (ed) 1991 *Semiconductors Group IV Elements and III–V Compounds* (Berlin: Springer)

[44] Vurgaftman I, Meyer J R and Ram-Mohan L R 2001 Band parameters for III–V compound semiconductors and their alloys *J. Appl. Phys.* **89** 5815–75 (Note that the values of *C* in the review article are one-tenth the values in the literature. This factor has been included in this work.)

[45] Han T-T, Fu Y, Wang S-M and Larsson A 2007 Structural analysis of dilute-nitride zinc blende $In_xGa_{1-x}N_yAs_{1-y}$ cluster by a semiempirical quantum chemistry study *J. Appl. Phys.* **101** 123707

[46] Medeiros-Ribeiro G, Bratkovski A M, Kamins T I, Ohlberg D A A and Williams R S 1998 Shape transition of germanium nanocrystals on a silicon (0 0 1) surface from pyramids to domes Science **279** 353–5

[47] Zhao Z M *et al* 2006 The challenges in guided self-assembly of Ge and InAs quantum dots on Si *Thin Solid Films* **508** 195–9

[48] Rao S S 1982 *The Finite Element Method in Engineering* (Exeter, UK: Wheaton) pp 203–29

[49] Tersoff J, Teichert C and Lagally M G 1996 Self-organization in growth of quantum dot superlattices *Phys. Rev. Lett.* **76** 1675–8

[50] Marchetti R, Montalenti F, Miglio L, Capellini G, De Seta M and Evangelisti F 2005 Strain-induced ordering of small Ge islands in clusters at the surface of multilayered Si–Ge nanostructures *Appl. Phys. Lett.* **87** 261919

[51] Schülli T U *et al* 2009 Enhanced relaxation and intermixing in Ge islands grown on pit-patterned Si(0 0 1) substrates *Phys. Rev. Lett.* **102** 025502

[52] Capellini G, De Seta M, Evangelisti F, Zinovyev V A, Vastola G, Montalenti F and Miglio L 2006 Self-ordering of a Ge island single layer induced by Si overgrowth *Phys. Rev. Lett.* **96** 106102

[53] Medeiros-Ribeiro G and Williams R S 2007 Thermodynamics of coherently-strained Ge_xSi_{1-x} Nanocrystals on Si(0 0 1): alloy composition and island formation *Nano Lett.* **7** 223